JOURNAL OF MATERIALS SCIENCE 22 (1987) 351–355

The role of thermal contraction stresses associated to inclusions in the formation of the final microstructure of weld metal deposits

M. FERRANTE, K. AKUNE, M. ODAINAI
Universidade Federal de São Carlos, Departamento de Engenharia de Materiais, 13560 – São Carlos, SP – Brasil

The effect of deoxidation products on the formation of the final microstructure of weld deposits has been studied on a ferritic–austenitic stainless steel. Results show that the product phase austenite nucleates on dislocations set up by thermal contraction stresses. The presence of these defects has been ascertained by transmission electron microscopy and calculation confirms the existence of a plastic zone which surrounds the inclusions. This mechanism seems to be more effective than the direct nucleation of the second phase on the inclusion interface and has important implications for the problem of acicular ferrite formation in carbon steels.

Nomenclature

α = mean linear coefficient of thermal expansion over the given temperature range
E = Young's modulus
ν = Poisson's ratio
Y_2 = yield stress of matrix
R = distance from inclusion centre
R_1 = radius of inclusion
R_2 = outer radius of the elastic zone of matrix
R' = outer radius of the elasto-plastic zone of matrix
T = temperature change (increase is positive)

1. Introduction

The need to reconcile high strength levels with acceptable toughness gave origin to a series of investigations aimed at a better understanding of the structure–properties relationship in ferritic weld metal. The results of such studies revealed that acicular ferrite is the microconstituent giving the best combination of strength and toughness. Other investigations tried to optimize metal chemistry and process parameters, in terms of a microstructure containing a high proportion of acicular ferrite.

In this context, a number of investigators have recently become aware of the importance of oxygen levels, or more precisely, the nature, volume fraction and size distribution of deoxidation products. The theories so far proposed can be classified along two main lines, both relying on the effect of such inclusions upon hardenability:

(i) direct nucleation–oxygen-rich inclusions act as nucleants for intragranular ferrite [1]

(ii) austenite grain size control–oxides interact with the boundaries of the austenite grains thus controlling their final size [2]; as a consequence the $\gamma \rightarrow \alpha$ transformation temperature is altered and so is the resulting microstructure.

The above models have been tested by several investigators whose results and conclusions were recently summarized [3], the general trend being a confirmation of the importance of oxygen content on both microstructure and toughness properties of weld metal. However, further work is still necessary since a number of uncertainties can be pointed out. For instance the pinning mechanism was criticized on the basis that most of the studies confirming it have been made on reheated weld metal [4]. Also, some investigators reported a constant austenitic grain size giving different final microstructures [5, 6].

Regarding the direct nucleation model, its maximum effectiveness is related to a certain size distribution when other factors are kept constant. Low oxygen content means an insufficient number of intragranular nucleation sites while high oxygen levels imply coarser inclusions, which are ineffective for acicular ferrite nucleation [1]. However recent studies on oxide inclusion size distribution have shown that there is only a weak correlation between average inclusion diameter and oxygen content. Pargeter [7] for instance, studied some 20 welds and found that although the oxygen level was in the range of 190 to 1550 p.p.m. inclusion size distribution appeared to peak between 0.5 and 0.75 μm in all cases. It is then difficult to interpret the coarse microstructures associated with high oxygen content on the basis of the direct nucleation model only.

Watson proposed that since manganese is taken out of solution by the inclusions, a decrease of hardenability results [8]. It can be argued that deoxidation reactions occur under a vigorous stirring due to the arc, plus gas evolution and thermal currents which would ultimately cause the homogenization of such depletion. These remarks help to explain recent analytical scanning transmission electron microscope observations which have shown no detectable variation in either manganese or silicon around oxide inclusions [9, 10].

0022–2461/87 $03.00 + .12

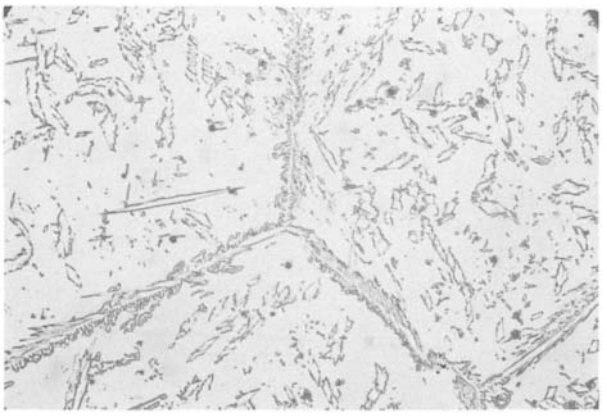

Figure 1 Light optical micrograph of the 26 Cr–5 Ni alloy. Solution treatment (1300° C, 30 min), isothermal transformation (800° C, 5 min) and air cooling. Magnification × 150.

The aim of the present work is to examine the validity of an alternative hypothesis regarding the role of deoxidation products, recently proposed by Harrison [11]. It is a modification of the direct nucleation model and is based on the assumption that the total austenite–inclusion interfacial area is insufficient to account for the observed changes in hardenability. In fact, some recent data show that weld metal with an oxygen content of 300 p.p.m. exhibits an inclusion–matrix total interfacial area of about 44 $mm^2 mm^{-3}$, which according to Harrison corresponds to the grain boundary area of a typical weld metal. It must be emphasized here that analysis of the inclusion size distribution [12] shows that about half of the interfacial area is made up by the larger particles (1.0 to 2.0 μm) which correspond to only 10 % of the total of inclusions. In other words nucleation sites are scarcer than indicated by inclusion–matrix total interfacial area considerations.

It was thus proposed that differences in thermal contraction between deoxidation products and austenite during cooling can originate stresses capable of exceeding the matrix yield point. The resulting dislocations would thus act as nucleation sites which surround the inclusions and ultimately increase the "volume" available for heterogeneous nucleation.

The present investigation attempts to test the above hypothesis, and discusses its relevance to acicular ferrite formation. An alloy other than Fe–C had to be chosen since the $\gamma \rightarrow \alpha$ reaction would obliterate any eventual substructure formed in the austenite. A duplex stainless steel was selected in the expectation that the final microstructure would allow observation both of direct nucleation events and of the matrix in the vicinity of the oxide inclusions.

2. Experimental procedure

One 6 Kg ingot was vacuum melted in an induction furnace. After hot rolling the alloy was drawn to a diameter of 3.5 mm in order to be used as consumable for the subsequent weld operation. Weld beads were obtained by submerged arc with a nominal heat input of 2.8 kJ mm^{-1} on a AISI 304 steel base plate. Dilution effects were minimized by depositing a total of four passes; the chemical composition of the top run was 23.3 wt % chromium, 5.7 wt % nickel, 1.6 wt % manganese.

After annealing at 1300° C for 60 min, a solution treatment at 1300° C for 30 min was necessary to dissolve the austenite and carbides; all the heat treatments were performed in a tube furnace under inert gas protection. Samples were then directly quenched to 800° C in a salt bath for 5 min in order to allow precipitation of austenite from the ferritic matrix.

Specimens for optical microscopy were mechanically polished and electrolytic etching was performed using aqueous 40% Na(OH) at 10 V. Thin foils for transmission electron microscopy were prepared from 3 mm discs of the weld metal. The discs were ground to 0.1 mm thickness and thinned in a Tenupol unit using a mixture of 5% perchloric/95% acetic acid at room temperature and at a potential of 30 V.

Quantitative microanalysis of the deoxidation products was performed on a Cambridge scanning electron microscope equipped with a Link Systems 860 microanalyser. All samples for optical microscopy, electron microscopy and microanalysis were taken from the top weld deposit, with the exception of the one shown in Fig. 1.

3. Results

A typical microstructure of the alloy after isothermal heat treatment is shown in Fig. 1. Austenite has precipitated both at ferrite grain boundaries and intragranularly. Some large inclusions are also visible and the austenite volume fraction is of the order of 33%. Fig. 2 shows some nucleation events, which are

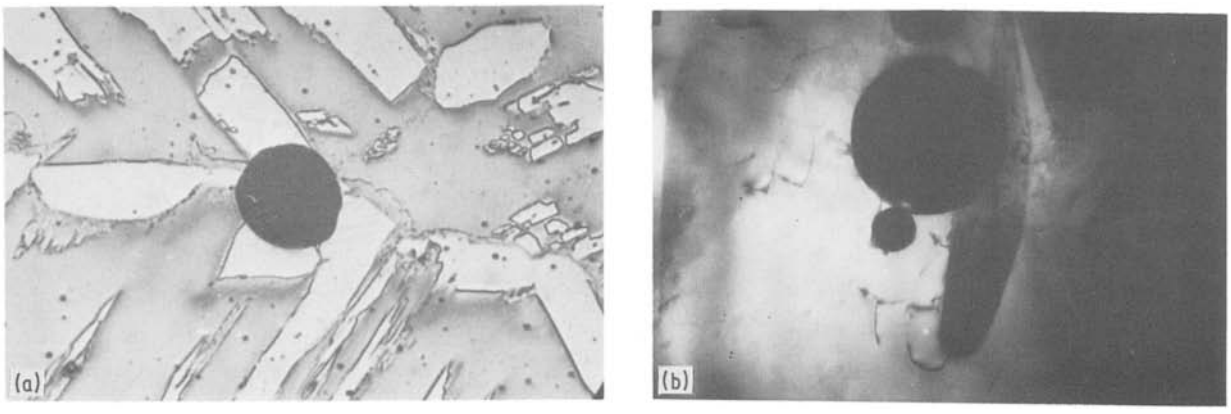

Figure 2 (a) Light optical micrograph of the top weld deposit showing a typical example of direct nucleation of austenite. Magnification × 400. (b) Transmission electron micrograph of a similar event. Magnification × 28 800.

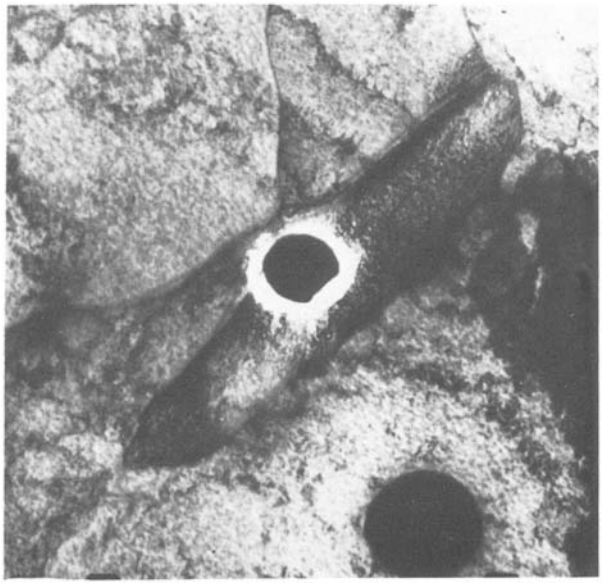

Figure 3 Transmission electron micrograph of a ferritic steel weld metal, illustrating nucleation of acicular ferrite on a deoxidation product. Taken from [12]. Magnification × 14 400.

perfectly analogous to those occurring in ferritic weld metals, see Fig. 3.

Transmission electron microscopy shows that deoxidation products are almost invariably associated with dislocation arrays and dislocation loops indicating the occurrence of plastic flow (Fig. 4). It must be pointed out that since the inclusions are quite large when compared to the foil thickness, these dislocations could simply be the consequence of foil relaxation during preparation of the samples. A separate experiment was therefore performed in order to decorate the supposedly preexisting dislocations with α' precipitates. These particles are a common occurrence both in high-chromium ferritic steels and duplex stainless steels when heated in the temperature range 400 to 600° C [13]. The experiment consisted of a 5 min anneal at 500° C followed by air cooling. Precipitation is evident in Fig. 5.

The composition of deoxidation products is presented in Table I. The analysis was performed on a large inclusion but only minor differences were observed if smaller inclusions were selected ($\sim 1.0\,\mu$m). From the data it can be assumed that the deoxidation products are of the type $MnOAl_2O_3SiO_2$.

TABLE I Mean inclusion composition (wt %)

Al	Si	Cr	Mn	Fe	O(balance)
7.7	24.8	3.1	21.0	1.5	41.9

4. Discussion

It has been shown that oxide inclusions act as nucleation sites for austenite in a 26 Cr–5 Ni ferritic stainless steel. These events resemble those occurring in Fe–C–Mn steel welds, with important implications for acicular ferrite nucleation since it is expected that a similar mechanism is involved in both cases.

Results also show that microstresses do develop around inclusions and the observed dislocation arrays indicate that the matrix yield point was exceeded. The role of dislocations on nucleation is well known: for example, Ramirez and Pound [14] calculated that at a supersaturation of $480\,J\,mol^{-1}$ and for an interfacial energy of $0.24\,J\,m^{-2}$ the barrier for homogeneous nucleation is 7.06 eV while for nucleation at screw and edge dislocations it is 1.60 and 0.93 eV respectively.

As mentioned in the Introduction, these defects are assumed to arise from thermal contraction stresses which are of the general form:

$$\Phi \pm \Phi(\alpha_2 - \alpha_1)T$$

where Φ is a function of the elastic moduli of the inclusion and matrix, and of inclusion shape, size and distribution; α_1 and α_2 are the thermal expansion coefficients of the inclusion and matrix respectively, while T is the temperature change. Brooksbank and Andrews [15] developed a number of expressions which permit the calculation of stresses around a spherical inclusion in elasto-plastic matrix, based on a classical treatment due to Laszlo [16].

The expression for reduced shear stress (equal to twice the maximum shear stress) is given below. Its main assumption is that stress is zero at the inclusion provided its reduced shear stress is higher than that of the matrix. The symbols are explained in the Appendix.

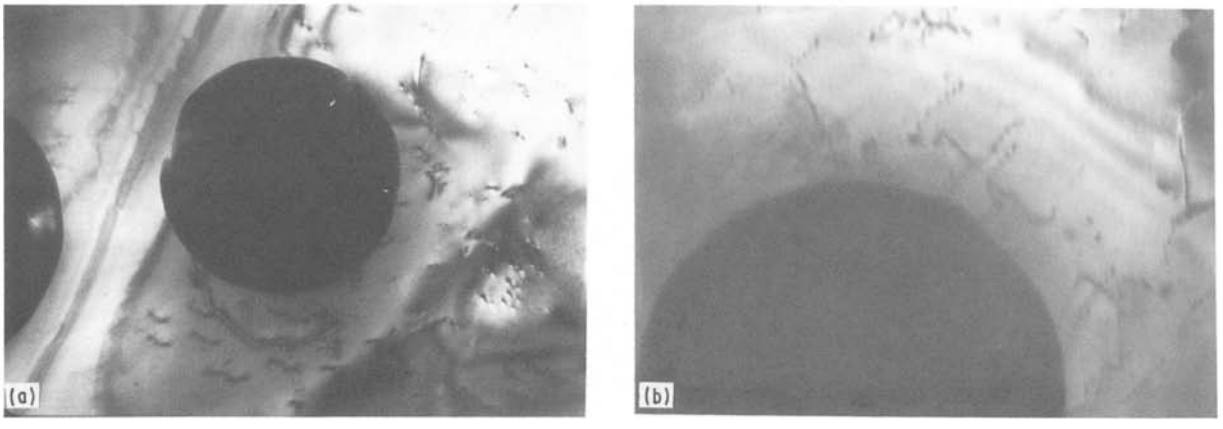

Figure 4 Transmission electron micrographs showing weld metal inclusions surrounded by dislocations and dislocation loops. Magnification (a) × 28 000 (b) × 42 500.

Figure 5 Transmission electron micrograph showing precipitation of particles on dislocations. Magnification × 53 000.

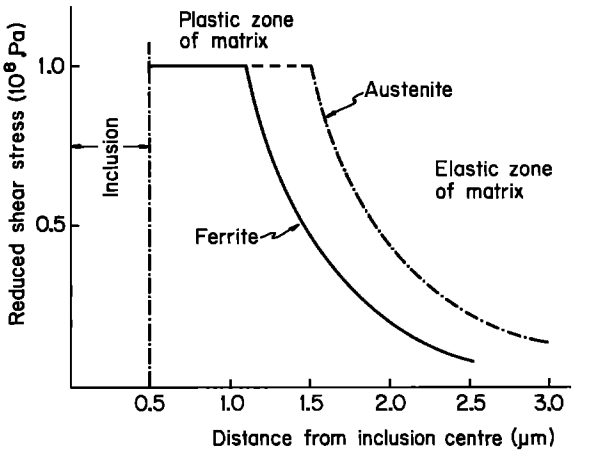

Figure 6 Stress distribution around a spherical inclusion.

$$F_1 = 0 \qquad (0 < R < R_1) \quad \text{Inclusion}$$

$$F_2 = \begin{cases} Y_2 & (R_1 < R < R') \\ & \text{Plastic zone of matrix} \\ Y_2\left(\dfrac{R'}{R}\right)^3 & (R' < R < R_2) \\ & \text{Elastic zone of matrix} \end{cases}$$

$$\left(\frac{1-2\nu_2}{E_2} - \frac{1-2\nu_1}{E_1}\right)\left[3 \ln \frac{R'}{R_1} + (1 - h^3)\right] = \frac{3}{2}\left[(\alpha_2 - \alpha_1)\frac{T}{Y_2} + \left(\frac{1-\nu_2}{E_2}\right)\left(\frac{R'}{R_1}\right)^3\right]$$

$$h = \frac{R'}{R_2}$$

The relevant physical constants are listed in Table II; subscript 1 refers to inclusion and 2 to matrix.

The above equations were employed to calculate the reduced shear stress for both ferritic and austenitic matrix containing a dispersion of $Al_2O_3SiO_2MnO$ inclusions. Results can be seen in Fig. 6, which plots reduced shear stress against distance from the inclusion centre. For a ferritic matrix the plastic zone extends to a distance that is almost equal to the inclusion radius, R_1. For the austenitic matrix such distance is $1.5R_1$. The operation of differential thermal stresses is supported by the agreement between the former theoretical results and the microstructural observations.

Obviously, the uncertainty concerning the physical constants of the matrix and inclusion at the transformation temperature somewhat limits the validity of the calculated results. However most of the deoxidation products which are typical of weld metal exhibit thermal expansion coefficients and elastics moduli leading to the development of residual stresses on cooling [15].

Besides the nucleation effect, dislocations can aid the austenite decomposition by enhancing carbon diffusion along its core thus increasing the effective diffusion coefficient of that element.

In the context of the mechanism proposed here, elastic moduli and thermal expansion coefficients of both matrix and inclusions are considered to be of primary importance with respect to the final microstructure. That being so, it would be useful to test the present model against still unexplained experimental results concerning the microstructure of ferritic steel weld metal.

Bhatty and co-workers [10] have recently attempted to explain the final microstructure of API 5LX65 steel weld metal in terms of the nature and distribution of oxide inclusions. They examined 16 different welds with almost identical chemical composition, and oxygen levels in the range 210 to 510 p.p.m. Acicular ferrite volume fraction varied from 85 to 16% and the deoxidation products consisted of a mixture of aluminium-rich inclusions and manganese-rich inclusions. The following points of their work will be discussed here:

(i) the percentage of acicular ferrite is virtually independent of oxygen levels

(ii) the acicular ferrite content decreases with the increase of the average manganese–aluminium ratio – their Fig. 11, here reproduced as Fig. 7.

The authors conclude that the results "do not give an insight into the basic mechanisms in terms of base metal chemistry, flux and welding wire combinations that have contributed to weld metal microstructure variations" and they finally suggest that the inclusions' efficiency as nucleants of acicular ferrite is related to their structure and composition.

The above results and conclusions can be rationalized in terms of the thermal contraction model. It must be noted that the inclusions denominated by Batty [10] as "manganese-rich" are a mixture of MnO

TABLE II Values of physical constants used in shear stress calculations (mks units)

Symbol	Inclusion	Reference	Ferrite matrix	Reference	Austenite matrix	Reference
ν	1/3		1/3		1/3	
E	2×10^{11}	[17]	5×10^{10}	[18]	5×10^{10}	[17]
α	2×10^{-6}	[15]	18×10^{-6}	[15]	22×10^{-6}	[15]
R	5×10^{-7}	[12]	1.3×10^{-5}	[12]	1.3×10^{-5}	[12]
Y	–	–	1×10^8 (800° C)	[15]	1×10^8 (500° C)	[20]

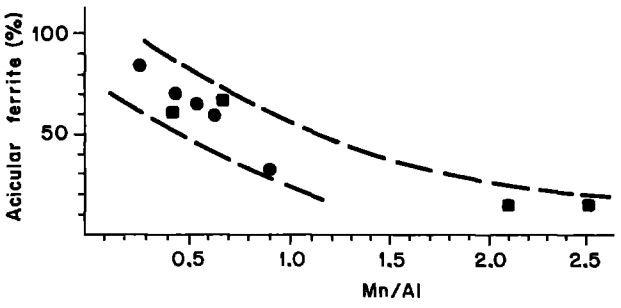

Figure 7 Acicular ferrite content versus Mn/Al ratios. Taken from [10]. (●) Calcium-free plate, (■) calcium-treated plate.

and SiO_2, as would be expected from their weld metal composition and the high deoxidation potential of silicon. Thus, the law of mixtures must be assumed as valid for inclusions composed of MnO and SiO_2.

Applying the same equations with the values in Table III the extension of the elasto-plastic zone in austenite can be calculated in terms of the distance from the inclusion centre and R/R' (Table IV). These results show that the plastic zone around manganese-rich inclusions is 30% smaller than the same zone associated to aluminium-rich inclusions, which is equivalent to a volume difference of about 50%.

Taking the volume of the plastic zone as a measure of the efficiency of the nucleation site it is possible to interpret the behaviour of Fig. 7 which clearly shows a decrease of acicular ferrite volume fraction with the increase of the proportion of manganese-rich inclusions. In fact the plastic zone of these inclusions has half the volume of the plastic zone associated to the alumina inclusions. Obviously this effect is a consequence of the thermal contraction mechanism and is independent of the overall oxygen content.

5. Conclusions

1. Deoxidation products act as nucleants for austenite precipitation in duplex stainless steel weld deposits. This mechanism is still under discussion in the context of acicular ferrite nucleation in ferritic steel weld metal.

2. Observations show that oxide inclusions are surrounded by dislocation networks extending to a distance comparable to their radius.

3. The dislocations are caused by stresses arising from differential thermal contraction between oxide and matrix. Calculations show that the plastic zone around the particles extends to a distance of about $1R_1$ and $1.5R_1$ for ferritic and austenitic matrix, respectively. In the former case there is a satisfactory agreement between microstructural observations and theoretical calculations.

4. Dislocation networks seem to be more effective as nucleation sites than the inclusion–matrix interface. Thus the present model can be understood as a reinterpretation of the direct nucleation model proposed by Abson, Dolby and Hart [1].

5. The application of the thermal contraction model to a series of experimental data taken from the literature shows that the proportion of acicular ferrite is correlated to the size of the plastic zone surrounding the inclusions.

TABLE III Values of physical constants (mks units)

Symbol	Al_2O_3	Reference	$MnOSiO_2$	Reference
ν_1	0.25	[15]	0.33	[21, 22]
E_1	4×10^{11}	[15]	9.7×10^{10}	[21, 22]
α_1	8×10^{11}	[15]	1.1×10^{-5}	[21, 22]
R_1	5×10^{-7}	[12]	5×10^{-7}	[12]

TABLE IV Size of plastic zone surrounding inclusions

	$MnOSiO_2$*	Al_2O_3
Distance (μm)	1.1	1.4
R/R'	2.2	2.7

*This oxide was assumed to have a crystalline structure. From the weld metal compositions studied by Bhatty and co-workers it was concluded that the SiO_2/MnO ratio was insufficient to promote the vitreous state.

References

1. D. J. ABSON, R. E. DOLBY and P. H. HART, in International Conference on "Trends in Steels and Consumables for Welding" (The Welding Institute, London, 1978) p. 75.
2. R. C. COCHRANE and P. R. KIRKWOOD, *ibid.*, p. 103.
3. B. AHBLOM, International Institute of Welding IX-1322-84 (1984).
4. R. A. RICKS, P. R. HOWELL and G. S. BARITTE, *J. Mater. Sci.* **17** (1982) 723.
6. H. TERASHIMA and J. TSUBOI, *Met. Constr.* **14** (1982) 472.
7. R. J. PARGETER, The Welding Institute Research Report no. 151/1981, July 1981.
8. M. N. WATSON, PhD thesis, University of Southampton, Southampton (1980).
9. G. S. BARITTE, R. A. RICKS and P. R. HOWELL, in Proceedings of Conference on Quantitative Microanalysis with High Spatial Resolution, Manchester, (1981) p. 112.
10. A. R. BHATTY, M. E. SAGGESE, D. N. HAWKINS, J. A. WHITEMAN and M. S. GOLDING, *Weld. J.* **63**, (7) (1984) 224-s.
11. P. L. HARRISON, Southampton University Report ME 79/24, October 1979.
12. M. FERRANTE and R. A. FARRAR, *J. Mater. Sci.* **17** (1982) 3293.
13. P. D. SOUTHWHICK and R. W. K. HONEYCOMBE, *Met. Sci.* **14** (1980) 254.
14. R. GOMEZ-RAMIREZ and G. M. POUND, *Met. Trans.* **4** (1973) 1563.
15. D. BROOKSBANK and K. W. ANDREWS, *J. Iron and Steel Inst.* **210** (1972) 246.
16. F. LASZLO, *ibid.*, **152** (1945) 207.
17. J. I. MUELLER *et al.* (eds) "Design with Brittle Materials", University of Washington (1979).
18. H. J. FROST and M. F. ASHBY, in "Fundamental Aspects of Structural Design", edited by R. I. Jaffe & B. A. Wilcox (Plenum Press, New York, 1977).
19. C. M. SELLARS, J. P. SAH, J. BENYON and S. R. FOSTER, SRC Report B/RG/1981 (1981).
20. R. J. TRUMAN, R. P. HARVEY, R. F. JOHNSON and J. N. SMITH, in Proceedings of the BISRA and ISI Conference on High Temperature Properties of Steels, Eastbourne, April 1966.
21. Engineering Properties Data on Selected Ceramics. Vol. 3, Batelle Columbus Laboratories, Metals and Ceramics Information Center, Report, July 1981.
22. Engineering Properties of Selected Ceramic Materials (The American Ceramic Society, Columbus, Ohio, 1966).

Received 27 February
and accepted 22 May 1986